Atmos. Chem. Phys. Discuss., 14, 28523–28569, 2014
www.atmos-chem-phys-discuss.net/14/28523/2014/
doi:10.5194/acpd-14-28523-2014

Atmospheric Chemistry and Physics Discussions

Connecting the solubility and CCN activation of complex organic aerosols: a theoretical study using the Solubility Basis Set (SBS)

I. Riipinen[1,2], **N. Rastak**[1], **and S. N. Pandis**[2,3]

[1]Department of Applied Environmental Science, Stockholm University, Stockholm, Sweden
[2]Center of Atmospheric Particle Studies, Carnegie Mellon University, Pittsburgh, PA, USA
[3]Department of Chemical Engineering, University of Patras, Patras, Greece

Received: 26 October 2014 – Accepted: 27 October 2014 – Published: 17 November 2014

Correspondence to: I. Riipinen (ilona.riipinen@itm.su.se)

Published by Copernicus Publications on behalf of the European Geosciences Union.

Abstract

We present a theoretical study investigating the cloud condensation nucleus (CCN) activation of multicomponent organic mixtures. We modeled these complex mixtures using the solubility basis set (SBS, analogous to the volatility basis set VBS), describing the mixture as a set of surrogate compounds with varying water-solubilities in a given range. We conducted Köhler theory calculations for 144 different mixtures with varying solubility range, number of components, assumption about the organic mixture thermodynamics and the shape of the solubility distribution, yielding approximately 6000 unique CCN-activation points. The results from these comprehensive calculations were compared to three simplifying assumptions about organic aerosol solubility: (1) complete dissolution at the point of activation, (2) combining the aerosol solubility with the molar mass and density into a single hygroscopicity parameter κ, (3) assuming a fixed water-soluble fraction $\varepsilon_{\mathrm{eff}}$. While the complete dissolution was able to reproduce the activation points with a reasonable accuracy only when the majority (70–80 %) of the material was dissolved at the point of activation, the single parameter representations of complex mixture solubility were confirmed to be powerful semi-empirical tools for representing the CCN activation of organic aerosol. Depending on the condensed-phase interactions between the organic molecules, material with solubilities larger than about 1–10 g L^{-1} could be treated as completely soluble in the CCN activation process over particle dry diameters between 20 and 500 nm and supersaturations between 0.03 and 8 %. Our results indicate that understanding the details of the solubility distribution in the range of 0.1 to 100 g L^{-1} is critical for capturing the CCN activation, while resolution outside this solubility range will probably not add much information except in some special cases. The connection of these results to the previous observations of the CCN activation of complex organic mixture aerosols is discussed.

ACPD
14, 28523–28569, 2014

1 Introduction

Interactions of atmospheric aerosol particles with ambient water vapour determine to a large extent the influence that aerosols have on climate. On one hand the water content of aerosol particles at atmospheric relative humidities (RH) below 100 % contributes significantly to the direct effect they have on the global radiative balance (Seinfeld and Pandis, 2006; Petters and Kreidenweis, 2007; Swietlicki et al., 2008; Zieger et al., 2011; Rastak et al., 2014). On the other hand the water-affinity of aerosol constituents, together with their dry size, defines the efficiency with which these particles can activate as cloud condensation nuclei (CCN) at supersaturated conditions (RH > 100 %), form cloud droplets, and thus affect the properties of clouds (Twomey, 1974; Aalbrecht et al., 1989; McFiggans et al., 2006). To quantify the effects of aerosol particles on clouds and climate it is thus necessary to understand the ways that aerosol constituents interact with water.

Organic compounds contribute a large fraction (20–90 %, depending on the environment) of atmospheric submicron particulate mass (Jimenez et al., 2009) – which is the part of the aerosol size distribution that typically dominates the CCN numbers. A significant fraction of this organic aerosol (OA) is secondary – i.e. produced in the atmosphere from the condensation of oxidation products of volatile, intermediate volatility and semi-volatile organic compounds (VOCs, IVOCs and SVOCs). Emissions of biogenic VOCs such as monoterpenes, isoprene and sesquiterpenes, their subsequent oxidation and condensation in the atmosphere are thought to be the dominant source of secondary organic aerosol (SOA) on a global scale (Hallquist et al., 2009 and references therein) – although recent studies indicate also a notable anthropogenic component to the global SOA (Volkamer et al., 2006; Hoyle et al., 2011; Spracklen et al., 2011).

The solubility in water is one of the key properties governing the water-absorption (i.e. hygroscopic growth) and CCN activation of aerosol particles. Together with the aqueous phase activity coefficients, surface tension and the dry mass of the particle,

ACPD
14, 28523–28569, 2014

water-solubility determines the aerosol particle water content in thermodynamic equilibrium (Pruppacher and Klett, 1997; Seinfeld and Pandis, 2006; Topping et al., 2012). Atmospheric organic compounds have a wide range of solubilities (Raymond and Pandis, 2003; Chan et al., 2008; Psichoudaki and Pandis, 2013). OA is thus a complex mixture of molecules with different CCN-behaviour as pure compounds. To accurately predict the water content and CCN activation of atmospheric OA, information on the dissolution behaviour and aqueous phase interactions of these complex mixtures is needed.

Representation of the complexity of OA is a major challenge for atmospheric chemical transport models: OA consists of thousands of different compounds whose properties are poorly known (Golstein and Galbally, 2007; Hallquist et al., 2009; Kroll et al., 2011). Approaches that simplify the complex nature of the OA mixture, yet reproducing its behaviour accurately enough, are required to assess the climate and air quality effects of atmospheric organics in large-scale modelling applications. One example of such approach is the representation of the condensation and evaporation of SOA using a limited number of surrogate compounds with a range of saturation concentrations, known as the volatility basis set (VBS, Donahue et al., 2006, 2011, 2012). Similar simplifying approaches are needed to represent the hygroscopic growth and CCN activation of OA as well.

When interpreting laboratory and field studies on hygroscopicity and CCN activation, a number of simplifying assumptions about the OA properties have been made, including: (1) assuming the organics to completely dissolve in water at the point of activation (Huff-Hartz et al., 2006), (2) assuming a fraction ($\varepsilon_{\mathrm{eff}}$) of organics to be completely soluble and the remaining fraction ($1-\varepsilon_{\mathrm{eff}}$) completely insoluble in water (Pruppacher and Klett, 1997; Engelhart et al., 2008), (3) lumping the solubilities, activity coefficients, molar masses and densities of the OA constituents into a single hygroscopicity parameter κ, which ranges between 0 and 1, and relates the water activity in the aqueous solution with the water and dry aerosol volumes (Petters and Kreidenweis, 2007, 2008, 2012;

ACPD
14, 28523–28569, 2014

Petters et al., 2009a, b, c). These common simplifications of organic aerosol solubility and hygroscopicity are summarized in Table 1.

Laboratory studies on different types of organic aerosols have provided important insights into the relationship between CCN-activation, hygroscopic growth and water-solubility of the atmospheric OA constituents. Raymond and Pandis (2002, 2003) and Chan et al. (2008) investigated the CCN activation of single- and multi-component aerosol particles consisting of organic compounds with known solubilities in water, and found that the particles activated at lower supersaturations than would have been expected based on the bulk solubility of their constituents. As an example, the laboratory studies by Chan et al. (2008) indicate that the CCN activation of material with water solubility as low as $1\,g\,L^{-1}$ could be predicted assuming complete dissolution. For some model systems the surface properties (wettability) of the aerosol particles, instead of the bulk water-solubility, seemed a more important factor defining their CCN activation (Raymond and Pandis, 2002). Huff-Hartz et al. (2006) assigned part of this effect to residual water left in the particles upon their generation, causing the particles to exist in metastable aqueous solutions and thus activate at lower supersaturations than the corresponding dry material. The rest of the apparent increase in solubility was assigned to potential impurities in the particles. In general the results reported by Huff-Hartz et al. (2006) suggested that compounds with water-solubilities above $3\,g\,L^{-1}$ behaved as if they were completely soluble in water.

Secondary organic aerosol particles generated in laboratory through oxidation chemistry and condensation of the reaction products have also been found to activate as cloud droplets and thus contribute to the atmospheric CCN budgets (Cruz and Pandis, 1997, 1998; Huff Hartz, 2005; VanReken et al., 2005; Prenni et al., 2007; King et al., 2007, 2009; Engelhart et al., 2008, 2011; Asa-Awuku, 2009, 2010). These particles probably resemble the real atmospheric SOA more closely than individual organic species or their simple mixtures, but the theoretical interpretation of their CCN-behaviour is complicated by the variety of their constituents. Despite the fact that CCN-activity of SOA has been reported to vary with e.g. the volatile precursor identity and

ACPD
14, 28523–28569, 2014

loading (Varutbangkul et al., 2006; King et al., 2009; Good et al., 2010), photochemical ageing (Duplissy et al., 2008; Massoli et al., 2010), and temperature (Asa-Awuku et al., 2009), the hygroscopicity parameter κ values determined for different SOA types are remarkably similar, being typically around 0.1 for the overall SOA and 0.3 for the dissolved fraction extracted from the aqueous sample (Asa-Awuku et al., 2010; King et al., 2010). Similarly, Huff Hartz (2005) reported effective solubilities of as high as $100\,g\,L^{-1}$ for both mono- and sesquiterpene SOA – although both are known to consist of a range of compounds with different solubilities. These results demonstrate the importance of knowing the water-soluble fraction of SOA at varying conditions but suggest that its exact speciation is probably not necessary for predictive understanding of the CCN activity of SOA particles (Asa-Awuku et al., 2010; Engelhart et al., 2011). The κ values inferred from sub- or supersaturated conditions for the same SOA mixtures, on the other hand, are not always consistent, the sub-saturated κ values being typically lower than the super-saturated ones (Prenni et al., 2007; Duplissy et al., 2008; Wex et al., 2009; Topping et al., 2012). Multiple possible reasons for this have been presented in the literature, including incomplete dissolution of the aerosol constituents at sub-saturated conditions (Petters et al., 2009a), surface tension effects (Good et al., 2010), RH-driven effects on the reaction chemistry and thus the composition (solubility and activity) of the formed SOA (Poulain et al., 2010), evaporation and condensation of semi-volatile organic compounds (Topping et al., 2012), or the non-ideality of the mixtures being more pronounced at the sub-saturated conditions (Kreidenweis et al., 2006; Petters et al., 2009a; Good et al., 2010).

While the basic theory of cloud droplet activation for pure water-soluble compounds is relatively well-established (Pruppacher and Klett, 1997; Asa-Awuku et al., 2007; Topping et al., 2012), and a number of theoretical and experimental studies on the different aspects controlling the CCN-activation of SOA have been presented (see above, McFiggans et al., 2006; Dusek et al., 2006 and references therein), only few of these studies have investigated the implications of the water-solubilities of complex organic mixtures on CCN activation. Understanding the relationship between the dissolution

ACPD
14, 28523–28569, 2014

behaviour and CCN-activation of complex organic mixtures is, however, needed to constrain the water-soluble fraction of SOA in varying conditions as well as to systematically unravel the mechanisms causing the apparent simplicity in the CCN-behaviour of complex organic mixtures.

In this work we introduce a framework (Solubility Basis Set, SBS) representing the mixture components with a continuous distribution of solubilities, similar to the VBS (Donahue et al., 2006, 2011, 2012). Using this framework in a theoretical model, we investigate the dissolution behaviour of complex organic mixtures and their CCN activity. In particular, we study the response of the CCN-activation to varying solubility ranges, distributions, and numbers of components in the mixture. Furthermore, we compare the CCN-activation predictions using the simplified solubility representations outlined above (complete dissolution, soluble fraction $\varepsilon_{\mathrm{eff}}$, and hygroscopicity parameter κ) with the more detailed description using the full solubility distributions, and study the relationship of the simplified solubility parameters $\varepsilon_{\mathrm{eff}}$ and κ to the true mixture solubility. Although the solubility ranges and other thermodynamic properties of the mixture have been chosen to represent SOA, many of the concepts and approaches introduced here can be applied to any particles consisting of complex mixtures of organic compounds with varying water-solubilities.

2 Methods

2.1 Theoretical predictions of CCN activation of complex organic mixtures

Figure 1 schematically summarizes the model system considered in this study. We consider a monodisperse population of spherical aerosol particles consisting of an internal mixture of organic compounds. When exposed to water vapour, these particles grow reaching thermodynamic equilibrium between the water vapour and the particle phase. The wet particle is allowed to consist of maximum two phases: the insoluble organic phase and the aqueous phase. The compositions of the organic and aqueous

ACPD
14, 28523–28569, 2014

phases are determined on the one hand by the equilibrium between the aqueous phase and the water vapour, and on the other hand by the equilibrium of the aqueous phase with the organic insoluble phase. To isolate the effects of solubility from organic volatility effects, we do not allow the organics to evaporate from the droplet – i.e. we assume that the equilibrium vapour pressures of the organics is zero above the droplet surface. Similarly, no condensation of organics from the gas phase to the particles is allowed to take place. This assumption is justified to a first order by the different equilibration time scales of the droplets with respect to water vapour and the organic vapours in typical atmospheric conditions. However, testing this assumption deserves some future attention, as also highlighted by Topping et al. (2012). The organic composition and dry particle size were treated as an input to a model calculating the final equilibrium composition, wet size, and CCN activation behaviour of these particles. Note that while the solubility enters the equations presented in the next Sects. 2.1 and 2.2 in the non-dimensional units of $g\,g^{-1}_{H_2O}$, in the presentation of the results it is converted into $g\,L^{-1}$, assuming constant unit density of water.

2.1.1 Equilibrium between water vapour and a mixed organic particle

The Köhler equation (Pruppacher and Klett, 1997) is used to link the ambient water vapour saturation ratio S with the size, composition and water content of the aerosol particles in thermodynamic equilibrium (lower panel of Fig. 1):

$$S = \frac{p_{\mathrm{w,\,eq}}}{p_{\mathrm{w,\,sat}}} = a_{\mathrm{w}} \exp\left(\frac{4\sigma M_{\mathrm{w}}}{RT\rho D_{\mathrm{p,\,wet}}}\right), \quad (1)$$

where $p_{\mathrm{w,\,eq}}$ (Pa) is the equilibrium vapor pressure of water over the droplet surface, $p_{\mathrm{w,\,sat}}$ (Pa) the saturation vapor pressure over a pure flat water surface, σ ($N\,m^{-1}$) is the surface tension of the droplet, M_{w} ($kg\,mol^{-1}$) the molar mass of water, ρ ($kg\,m^{-3}$) the density of the aqueous phase, $D_{\mathrm{p,\,wet}}$ (m) the diameter of the droplet, T (K) the temperature and R ($J\,mol^{-1}\,K^{-1}$) the universal gas constant. a_{w} is the water activity,

ACPD
14, 28523–28569, 2014

defined as the product of the water mole fraction X_w and water activity coefficient in the aqueous phase Γ_w:

$$a_w = X_w \Gamma_w. \quad (2)$$

The activity coefficient describes the interactions between water molecules and the dissolved organic molecules in the mixture. The saturation ratio at which the particles of dry size $D_{p,\,dry}$ activate as cloud droplets (i.e. continue growing in size even if the saturation ratio decreases), is referred to as the critical saturation ratio S_c. Mathematically this corresponds to the highest local maximum in the $S(D_{p,\,wet})$ curve, usually referred to as the Köhler curve.

2.1.2 Equilibrium between the aqueous and insoluble organic phases

The composition of the droplet and the distribution of material between the organic insoluble and the aqueous phases was calculated applying the principles of mass conservation and the equilibrium concentrations of the organic components in an aqueous mixture above the insoluble organic phase. As the mass transfer of organics between the particles and the gas phase is neglected, the total mass of the dry particle m_{dry}, being the sum over all components i, is equal to the total organic mass in the wet droplet (see Fig. 1):

$$m_{dry} = \sum_{i}^{n} m_{i,\,insoluble} + \sum_{i}^{n} m_{i,\,aqueous}, \quad (3)$$

where n is the total number of organic compounds, $m_{i,\,insoluble}$ is the mass of compound i in the insoluble organic phase and $m_{i,\,aqueous}$ the mass of compound i in the aqueous phase. The same holds for each organic compound individually:

$$m_{i,\,dry} = y_{i,\,dry} m_{dry} = m_{i,\,insoluble} + m_{i,\,aqueous}, \quad (4)$$

ACPD
14, 28523–28569, 2014

where $y_{i,\,\mathrm{dry}}$ is the mass fraction of i in the dry organic particle. On the other hand, the concentration of each organic compound in the aqueous phase is determined by the thermodynamics of the two-phase system consisting of the insoluble organic phase and the aqueous solution phase above it. The mass of each organic compound i in the aqueous phase can be expressed as:

$$m_{i,\,\mathrm{aqueous}} = \begin{cases} \gamma_i Y_{i,\,\mathrm{wet}} c_{\mathrm{sat,\,pure},\,i} m_{\mathrm{w}}, & Y_{i,\,\mathrm{wet}} > 0 \\ m_{i,\,\mathrm{dry}}, & Y_{i,\,\mathrm{wet}} = 0 \end{cases} \quad (5)$$

where γ_i is the activity coefficient of i in the insoluble organic phase, $Y_{i,\,\mathrm{wet}}$ and $c_{\mathrm{sat,\,pure},\,i}$ (here in $\mathrm{g\,g^{-1}_{H_2O}}$) are the organic phase mole fraction and pure component solubility (saturation concentration) of i, and m_{w} is the total mass of water. The former equation corresponds to the situation where the particle contains an insoluble organic core in thermodynamic equilibrium, the latter to the case where only the aqueous phase exists, i.e. all the organic material has dissolved to the water. In this study we assume a constant molar mass throughout the organic mixture for simplicity, leading to the mass and mole fractions in the organic phase to be the same, i.e. $Y_i = y_i$ for all the compounds. However, all the equations presented below can be re-derived in a relatively straightforward manner taking into account a potential difference between the mole and the mass fractions in the organic phase.

Finding the organic and aqueous phase compositions that satisfy Eqs. (3)–(5) for given water and dry particles masses (m_{w} and m_{dry}, respectively) requires solving n coupled equations. These equations were expressed using the ratio of organic compound i in the insoluble core of the wet particle to the total mass of the compound (Raymond and Pandis, 2003; Petters and Kreidenweis, 2008):

$$\chi_i = \frac{m_{i,\,\mathrm{insoluble}}}{m_{i,\,\mathrm{insoluble}} + m_{i,\,\mathrm{aqueous}}} = \frac{m_{i,\,\mathrm{insoluble}}}{m_{i,\,\mathrm{dry}}} = \frac{m_{i,\,\mathrm{insoluble}}}{Y_{i,\,\mathrm{dry}} m_{\mathrm{dry}}}. \quad (6)$$

ACPD
14, 28523–28569, 2014

The mole fraction (equal to the mass fraction for the mixtures considered here) of i in the insoluble core is defined as

$$Y_{i,\,\mathrm{wet}} = \frac{m_{i,\,\mathrm{insoluble}}}{\sum_i m_{i,\,\mathrm{insoluble}}} = \frac{\chi_i m_{i,\,\mathrm{dry}}}{\sum_i \chi_i m_{i,\,\mathrm{dry}}} = \frac{\chi_i Y_{i,\,\mathrm{dry}}}{\sum_i \chi_i Y_{i,\,\mathrm{dry}}}. \quad (7)$$

Finally, combining Eqs. (3)–(7), we get n equations of the form

$$\chi_i = 1 - \frac{\chi_i Y_{i,\,\mathrm{dry}} c_{i,\,\mathrm{sat,\,pure}} m_{\mathrm{w}}}{m_{i,\,\mathrm{dry}} \sum_i \chi_i Y_{i,\,\mathrm{dry}}}, \quad (8)$$

which can be solved for χ_i with the constraint $0 \le \chi_i \le 1$ for given water and dry particle masses.

2.1.3 Representation of complex organic mixtures: solubility distributions and thermodynamic properties

A novel aspect of this study as compared with previous theoretical work is the representation of complex mixtures using their aqueous solubility distribution, referred to as the Solubility Basis Set (SBS). In our calculations we used mixtures of n compounds, whose water-solubilities ranged from $c_{\mathrm{sat,\,min}}$ to $c_{\mathrm{sat,\,max}}$, either on a linear or logarithmic basis. The shape of the distribution could vary as well. In this work we studied essentially three types of mass fraction distributions in the dry particle: a uniform distribution in which all solubilities are equally abundant, distribution increasing steadily (linearly or logarithmically), and a distribution decreasing steadily (linearly or logarithmically). The 72 studied solubility distributions are specified in Table 2, and the solubility distributions for $n = 10$, $c_{\mathrm{sat,\,min}} = 0.1\,\mathrm{g\,L^{-1}}$ and $c_{\mathrm{sat,\,max}} = 1000\,\mathrm{g\,L^{-1}}$ are presented in Fig. 2 as examples.

For simplicity, we assumed that water forms an ideal solution with the dissolved organics, i.e. $\Gamma_{\mathrm{w}} = 1$, thus yielding an activity equal to the mole fraction of water, $a_{\mathrm{w}} = X_{\mathrm{w}}$

ACPD
14, 28523–28569, 2014

in Eq. (1). Since information about the activity coefficients of organic species in purely organic mixtures is still scarce, we studied two alternative approaches to represent the dissolution thermodynamics of the SOA mixture in Eqs. (9)–(12): (1) assuming an ideal mixture where $\gamma = 1$ for all compounds, (2) assuming a constant organic phase activity $\gamma_i Y_{i,\,\mathrm{wet}}$ of unity for all compounds – in which case the dissolution behaviour of each i is similar to their behaviour as pure components. These cases probably represent the limiting cases for the dissolution of SOA components in CCN activation reasonably well, the former representing a lower limit and the latter an upper limit for the overall solubility of the dry particle. Applying the two limiting assumptions about the interactions of the compounds in the organic phase for the 72 different solubility distributions (Table 2) thus results in total 144 unique representative model mixtures.

The density, surface tension, and molar masses assumed for water and the organic compounds are summarized in Table 3. Although the density, surface tension and molar mass of the organics are likely to vary with the solubility, we kept them constant throughout the organic mixture to isolate the solubility effects on the CCN behaviour. The values were chosen based on literature studies of the CCN behaviour of SOA (Engelhart et al., 2008; Asa-Awuku et al., 2010). The surface tension σ and density ρ of the aqueous mixture (used in Eq. (1) and when converting between particle mass and volume/diameter) were calculated as the mole- and mass-weighted averages of water and organic mixture properties, respectively. Furthermore, we assumed no dissociation of the organics in the aqueous phase.

2.1.4 Model calculations

We solved Eq. (8) for organic mixtures with the Matlab internal function *fsolve*, for varying water and dry particle masses m_w and m_dry, covering 50 different dry particle diameters between 20 and 500 nm. The calculations yielded the composition of the insoluble organic and the aqueous phase, and thus the mole fraction of water in the aqueous solution X_w. From these results the Köhler curves $S(D_{\mathrm{p,\,wet}})$ corresponding to each dry particle mass could be calculated using Eq. (1) (see Fig. 3a for an example of

ACPD
14, 28523–28569, 2014

the Köhler curves). The critical supersaturations s_c (defined as $S_c - 1$) corresponding to specific dry particle diameters $D_{p,\,dry}$ (termed also as activation diameters $D_{p,\,act}$ at a given saturation ratio S or supersaturation s) were determined from the maxima of the Köhler curves (see Fig. 3a). The temperature was assumed to be 298 K in all calculations. These calculations for the 144 unique organic model mixtures corresponded to 7200 Köhler curves yielding 5957 ($D_{p,\,act}$, s_c) pairs (activation points, see Fig. 3b). For the remaining 1143 curves no activation points were found with the given combinations of mixture properties and dry diameters. For comparisons with the simple solubility representations, the dissolved organic fraction defined as

$$\varepsilon = \frac{\sum m_{i,\,aqueous}}{m_{dry}} \tag{9}$$

was extracted from the model output.

2.2 Comparison of the full model output to simple solubility representations

To investigate the performance of the simple solubility representations given in Table 1 in reproducing the CCN activation of complex mixtures, we fitted the ($D_{p,\,act}$, s_c) data created by the full model using these simpler models. No fitting is required for the complete solubility approach. Using the obtained solubility parameters from the optimal fit and the corresponding simplified forms of the Köhler equation we then recalculated new ($D_{p,\,act}$, s_c) pairs and compared them to the predictions by the full model. Furthermore, we investigated the relationships between the true mixture solubility distribution and the simplified solubility parameters. The details of the approach used for each simple model are outlined below.

2.2.1 Complete dissolution

In the case where all of the organic material is assumed to completely dissolve at the point of activation, the calculation of the aqueous solution composition becomes trivial

ACPD
14, 28523–28569, 2014

as

$$m_{i,\,\mathrm{dry}} = m_{i,\,\mathrm{aqueous}} \tag{10}$$

for all the compounds, and the water mole fraction can simply be calculated based on the dry particle mass as

$$X_{\mathrm{w}} = \frac{\frac{m_{\mathrm{w}}}{M_{\mathrm{w}}}}{\frac{m_{\mathrm{w}}}{M_{\mathrm{w}}} + \frac{m_{\mathrm{dry}}}{M_{\mathrm{org}}}}, \tag{11}$$

where m_{w} is the water mass in the droplet, m_{dry} the dry particle mass (related to $D_{\mathrm{p,\,dry}}$ through the organic density ρ_{org}) and M_{org} the organic molar mass. The X_{w} calculated in this way was inserted into Eq. (1) to yield the corresponding ($D_{\mathrm{p,\,act}}$, s_{c}) predictions and was also applied for calculating the solution density and surface tension as mass-weighted averages of the water and pure organic values.

2.2.2 Hygroscopicity parameter κ

In many practical applications the water activity and the difference in the densities and molar masses of water and the dry material are expressed with a single hygroscopicity parameter κ, introduced by Petters and Kreidenweis (2007), defined as:

$$\frac{1}{a_{\mathrm{w}}} = 1 + \kappa\frac{V_{\mathrm{s}}}{V_{\mathrm{w}}}, \tag{12}$$

where V_{s} and V_{w} are the volumes of the dry material and water, respectively. The following formulation of the relationship between water saturation ratio, aerosol size and composition is referred to as the κ-Köhler equation:

$$S = \frac{D_{\mathrm{p,\,wet}}^3 - D_{\mathrm{p,\,dry}}^3}{D_{\mathrm{p,\,wet}}^3 - D_{\mathrm{p,\,dry}}^3(1-\kappa)} \exp\left(\frac{4\sigma M_{\mathrm{w}}}{RT\rho D_{\mathrm{p,\,wet}}}\right) \tag{13}$$

ACPD
14, 28523–28569, 2014

yielding an approximate expression for the relationship between s_c and $D_{p,\,act}$ defined as

$$s_c = \frac{2}{3}\left(\frac{4M_w\sigma}{RT\rho}\right)^{3/2}\left(3\kappa D_{p,\,act}^3\right)^{-1/2}, \quad (14)$$

Equation (14) was fitted to all ($D_{p,\,act}$, s_c) data produced for a given organic mixture composition (see Table 2) by the full model, thus assuming a constant κ value for a given organic mixture. To mimic the application of Eq. (14) to experimental data with no knowledge on the exact solute composition, in this case we assumed the surface tension and density to be those of water when fitting the κ values to the full model data.

2.2.3 Soluble fraction ε_{eff}

For an ideal solution of water and an organic solute the κ is directly proportional to the dissolved fraction and the ratio of the molar volumes of water and the solute i.e.: $\kappa = \varepsilon\kappa_{max}$, where $\kappa_{max} = M_w/M_{org}\cdot\rho_{org}/\rho_w$. Assuming that a single soluble fraction ε_{eff} can represent a given organic mixture (see Table 2) at all considered supersaturations, and substituting these relationships into Eq. (16) yields

$$s_c = \frac{2}{3}\left(\frac{4M_w\sigma}{RT\rho}\right)^{3/2}\left(3\frac{M_w}{M_s}\frac{\rho_s}{\rho_w}\varepsilon_{eff}D_{p,\,act}^3\right)^{-1/2}, \quad (15)$$

the corresponding form of the Köhler equation being (see Huff Hartz, 2005)

$$S = \frac{M_{org}\rho_w(D_{p,\,wet}^3 - D_{p,\,dry}^3)}{D_{p,\,wet}^3(M_{org}\rho_w) + D_{p,\,dry}^3(\varepsilon_{eff}M_w\rho_{org} - M_{org}\rho_w)}\exp\left(\frac{4\sigma M_w}{RT\rho D_{p,\,wet}}\right). \quad (16)$$

Again, we fitted Eq. (17) to the data produced by the full model and assumed the aqueous solution density and surface tension to be equal to those of water. When

ACPD
14, 28523–28569, 2014

$\varepsilon_{\mathrm{eff}} < 1$, the following relationship has been used to estimate the effective saturation concentration of the mixture (Raymond and Pandis, 2002; Huff Hartz, 2005)

$$c_{\mathrm{sat,\,eff}} = \frac{\rho_{\mathrm{w}}(D^3_{\mathrm{p,\,wet}} - D^3_{\mathrm{p,\,act}})}{\varepsilon_{\mathrm{eff}}\rho_{\mathrm{org}}D^3_{\mathrm{p,\,act}}}. \quad (17)$$

2.2.4 Connection between $\varepsilon_{\mathrm{eff}}$ and the solubility distribution of the mixture

Let us now assume that the dissolved fraction at the point of activation for each considered mixture can be expressed as a sum of two terms: the contribution from the compounds present in the potential insoluble core and the contribution of the compounds that are completely dissolved, i.e.

$$\varepsilon = \frac{\sum_{i=1}^{i_{\mathrm{t}}} m_{i,\,\mathrm{aqueous}} + \sum_{j=i_{\mathrm{t}}+1}^{n} m_{j,\,\mathrm{dry}}}{m_{\mathrm{dry}}} = F_{\mathrm{w}} \sum_{i=1}^{i_{\mathrm{t}}} \gamma_i Y_{i,\,\mathrm{wet}} c_{\mathrm{sat,\,pure},\,i} + \sum_{j=i_{\mathrm{t}}+1}^{n} Y_{\mathrm{dry},\,j}, \quad (18)$$

where

$$F_{\mathrm{w}} = \frac{m_{\mathrm{w}}}{m_{\mathrm{dry}}}. \quad (19)$$

We expect that the ε given by Eq. (18) represents the $\varepsilon_{\mathrm{eff}}$ yielded from the fits assuming a single constant soluble fraction for a given organic mixture. The key assumption made in Eq. (18) is that only compounds with pure component solubilities below a given threshold solubility c_{t} contribute to the potential insoluble core, while all the material above this threshold is completely dissolved at the point of activation. The index i_{t} denotes the solubility bin corresponding to c_{t}, and the value of i increases with increasing solubility.

Let us now explore the limiting cases for the dissolved fraction ε and its link to the solubility distributions in the studied mixtures. If nothing is completely dissolved $i_{\mathrm{t}} = n$

ACPD
14, 28523–28569, 2014

and ε is the cumulative sum of the solubilities present in the mixture weighted with the activities and F_w. Similarly, if everything is completely dissolved, $i_t = 0$. In the case where both terms in Eq. (18) are non-zero, the first term is always smaller than the second term – as the dissolved mass of any compound i cannot exceed the total mass of that compound, $m_{i,\,\mathrm{aqueous}} \leq m_{i,\,\mathrm{dry}}$. In this case, the threshold solubility c_t is thus found at the lowest bin where the two terms are comparable in magnitude, i.e.

$$\lim_{i \to i_t^-} F_w \gamma_i Y_{\mathrm{wet},\,i} c_{\mathrm{sat,\,pure},\,i} = Y_{\mathrm{dry},\,i}. \tag{20}$$

At the limit of large n, the threshold solubility c_t is thus found from the bin where

$$c_{\mathrm{sat,\,pure},\,i_t} = c_t \approx \frac{Y_{\mathrm{dry},i_t}}{Y_{\mathrm{wet},\,i_t}} \cdot \frac{1}{\gamma_{i_t}} \cdot \frac{1}{F_w}. \tag{21}$$

This is also equal to the bin where 50 % of the material is partitioned in the insoluble organic phase, i.e.

$$\chi_{i_t} = \frac{m_{i_t,\mathrm{insoluble}}}{m_{i_t,\mathrm{insoluble}} + m_{i_t,\mathrm{aqueous}}} = \frac{1}{1 + \frac{m_{i_t,\mathrm{aqueous}}}{m_{i_t,\mathrm{insoluble}}}} = \frac{1}{2}. \tag{22}$$

Equation (22) is analogous to the atmospheric gas-particle partitioning considerations for organic compounds using the VBS (Donahue et al., 2006). Similarly to the VBS approach for volatilities, one can thus define an effective saturation concentration in the aqueous phase

$$c^{\mathrm{eff}}_{\mathrm{sat},\,i} = Y_{\mathrm{wet},\,i} \gamma_i c_{\mathrm{sat,\,pure},\,i}, \tag{23}$$

yielding a simpler expression for the threshold solubility above which everything can be assumed to dissolve,

$$c^{\mathrm{eff}}_{\mathrm{sat},\,i_t} \approx \frac{Y_{i_t,\mathrm{dry}}}{F_w}. \tag{24}$$

ACPD
14, 28523–28569, 2014

While calculating the threshold volatility for the 50 % partitioning of atmospheric organics (expressed as the effective saturation concentration C^* in µg of organic compound in m^{-3} of air) requires knowledge on the total particulate mass suspended in air, finding the corresponding solubility threshold c_t requires knowledge of the total amount of organic material as compared with the water at the point of activation, manifested in the ratio F_w. F_w, on the other hand, depends on the ambient supersaturation and the total soluble mass – thus introducing a supersaturation-dependence to the ε given by Eq. (18) as well. The magnitude of F_w as a function of supersaturation can be estimated by substituting Eqs. 15 and 17 into the definition of F_w (Eq. 29) and after some rearranging, yielding:

$$F_w = \frac{\rho_w}{\rho_{org}} \left(\frac{2\varepsilon}{s_c} \cdot \frac{\rho_{org}}{\rho_w} \cdot \frac{M_w}{M_{org}} - 1 \right) = \frac{\rho_w}{\rho_{org}} \left(\frac{2\varepsilon\kappa_{max}}{s_c} - 1 \right). \quad (25)$$

3 Results

Figure 3a displays examples of the Köhler curves obtained from solving Eqs. 1 and 6 for distribution 1 (the flat logarithmic distribution) with varying solubilities and $n = 5$, assuming that the organics form an ideal mixture with each other. Each curve corresponds to a different dry size, and the dots indicate the activation point (S_{crit} corresponding to the activation dry diameter $D_{p,\,act}$). Black dots indicate incomplete dissolution ($\varepsilon < 0.99$) at the point of activation while red dots indicate that in practise all the organics are dissolved into the aqueous phase at the point of activation ($\varepsilon > 0.99$). Qualitatively similar behaviour was observed for all the considered distributions: as the overall solubility of the mixture increases, the dissolution of the compounds increases, leading eventually to complete dissolution at the point of activation. The transition from a regime with two phases (aqueous + insoluble) to single aqueous phase is visible in the two maxima in Fig. 3a, in accordance with Shulman et al. (1996) and Petters and Kreidenweis (2008).

ACPD
14, 28523–28569, 2014

Figure 3b illustrates the parameter space probed in this study, showing the 5957 (s_{crit}, $D_{p,\,act}$) points corresponding to the Köhler curve maxima calculated for all the considered organic mixtures. The relationships between the critical supersaturation, activation diameter, and dissolved fraction ε at the point of activation are also schematically shown. The chosen dry diameters and supersaturations represent a conservative range of typical atmospheric conditions – as the total aerosol number concentrations are dominated by ultrafine (diameters smaller than 100 nm) particles at most locations. In most considered cases the dissolved fractions fall between 0.1 and 1, but the lowest dissolved fractions at the point of activation are of the order of only a few percent – thus mimicking nearly insoluble aerosols. We therefore believe that the cases considered here represent a reasonable sample of atmospherically relevant conditions and SOA mixture compositions. The water-to-organic mass ratios F_w corresponding to the probed conditions and mixtures (see Sect. 2.2.4) range from values below 1 up to 1000, with most values around 10–100. In many of the following plots and considerations we have chosen four specific supersaturations, 0.1, 0.3, 0.6 and 1 %, as representative values for typical laboratory experiments, which are also indicated in Fig. 3b.

An example of the dependence of the activation diameter $D_{p,\,act}$ on the solubility range for all the studied distributions (see Table 2) and $n = 5$ is presented in Fig. 4. As expected, the activation diameter decreases with increasing supersaturation and solubility range for a given solubility distribution. The solubility distribution is reflected in the overall magnitude of the activation diameters: the distributions that have larger fractions of material in the higher end of the solubility range (distributions 2, 3, and 4) have generally lower activation diameters for a given supersaturation as compared with the other distributions. The case when unity activity in the organic phase is assumed results in smaller activation diameters for the same supersaturation as compared with the ideal organic mixture case.

Figure 5 presents the activation diameters predicted using the simplified solubility descriptions (Table 1) based on best fits to all available data as compared with the full description of the solubility distributions (Table 2). The results clearly show, not

ACPD
14, 28523–28569, 2014

surprisingly, that assuming complete dissolution for all the mixtures consistently under-predicts the activation diameters (Fig. 5a). Representing the dissolution behaviour with only one additional parameter, i.e. the hygroscopicity parameter κ (Eqs. 15 and 16) or the effective soluble fraction $\varepsilon_{\mathrm{eff}}$ (Eqs. 17 and 18) improves the agreement between the activation diameters considerably (Fig. 5b and c). Adding the knowledge about the molar mass and density of the organic mixture, which is the only difference between using the $\varepsilon_{\mathrm{eff}}$ instead of the single κ, adds only marginal improvements in predicting the activation diameters for a given supersaturation. The disagreements between the simplified models and the full theoretical treatment are largest for the smallest supersaturations. These are the cases with the widest range of possible ε values at the point of activation (see Fig. 3b), and the effect is most obvious for the complete dissolution model: the larger the deviation from complete dissolution at the point of activation (i.e. the $\varepsilon \sim 1$ case in Fig. 3b) the more significant error we introduce. The activation diameters predicted assuming complete dissolution are within 10 % of the correct values if the real dissolved fraction ε is larger than about 0.7–0.8 at the point of activation.

The performance of the simple solubility models for all the studied Köhler curves is summarized in Fig. 6: while the complete dissolution assumption results in systematic under-prediction (up to 40 %) of the activation diameter, the κ- and $\varepsilon_{\mathrm{eff}}$-based models are generally within 10 % (in most cases within 5 %) of the activation diameter predicted for the full solubility distribution representation.

Figure 7 compares the fitted parameters representing the mixture dissolution to the corresponding values inferred from the full mixture data for the 144 different mixtures. In Fig. 7a, the effective soluble fractions $\varepsilon_{\mathrm{eff}}$ are compared to the actual dissolved fractions ε at the point of activation for all the studied mixtures. While in the fits a single constant $\varepsilon_{\mathrm{eff}}$ has been assumed to represent a given mixture (see Eqs. 15 and 16), in reality ε varies with supersaturation (Eq. 9). Thus, while the fitted $\varepsilon_{\mathrm{eff}}$ for a given mixture correlates very well with the average ε over all activation points (the markers in Fig. 7a), the performance of the approach can vary considerably with supersaturation (the grey lines in Fig. 7a). In practice this means that describing a given complex mixture with

ACPD
14, 28523–28569, 2014

a fixed soluble fraction yields representative average dissolution behaviour, but does not guarantee correct solubility description for a specific s_c if fitted over a range of supersaturations. The corresponding comparison for the hygroscopicity parameter κ values describing the data are shown in Fig. 7b. A clear correlaction between the fitted κ and the average ε is observed as expected (see Sect. 2.2.3), but the variation of ε with supersaturation again adds scatter to the data – suggesting a dependence of κ on s_c. The maximum κ, on the other hand, is defined primarily by the molar masses and densities of the organics. For our mixtures with constant M_{org} and ρ_{org} the value of κ_{max} is 0.15, which is indicated in Fig. 7b. The points above this theoretical maximum are a result of using the pure water density instead of the mixture value in the Kelvin term of the Köhler equation (Eq. 16). These results thus suggest that the κ values of 0.1–0.2 typically observed for SOA particles (Duplissy et al., 2011) are controlled by the molar masses and densities of the SOA mixtures to a large extent and can result from quite different SOA mixtures in terms of their solubilities.

To illustrate the relationship of the fitted ε_{eff} to the dissolution of a given mixture, the partitioning between the aqueous and insoluble organic phase is presented in Fig. 8 for distribution 1 with the "low" solubility range and $n = 100$ at the point of activation when $s_c = 0.1\,\%$ (see Table 2). Figure 8a shows the partitioning for the case where ideal organic mixture has been assumed and Fig. 8b shows the corresponding data for the unity activity case (see Eq. 5). The point of 50 %-partitioning (c_t, Eqs. 20 and 21) is also shown. As described in Sect. 2.2.4 we expect c_t to be a reasonable estimate for the limit for complete dissolution, if the complex mixture is reduced into a two-component mixture of completely soluble and insoluble components. It should be noted, however, that the water content and ε of the droplet at the point of activation depend on supersaturation (see Eq. 25), causing also a dependence between c_t and s_c. Furthermore, Fig. 8 illustrates a difference in the solubility-dependence of the partitioning behavior for the two organic activity assumptions. The ideal mixture displays a symmetrical sigmoidal dependence around c_t. For the unity activity case, on the other hand, the

ACPD
14, 28523–28569, 2014

undissolved fraction is asymmetric around the 50 %-value – dropping rapidly to zero above c_t but approaching 1 asymptotically below c_t.

Figure 9 shows the distributions of the solubility bins containing the 50 %-partitioning points (c_t, Eqs. 20 and 21) on a decadal basis for the 5967 unique activation points studied, illustrating also the differences between the two assumptions about the organic phase activity. The c_t values for the ideal organic mixture (Fig. 9a, based on 2465 points) display a symmetrical distribution around the median value of about $10\,g\,L^{-1}$. Also, a modest dependence of c_t on the number of components is observed: the cases with 3 and 5 components display slightly higher c_t values as compared with the cases with larger n. This apparent dependence is probably due to the discrete nature of the solubility distributions in combination with the fact that for the different solubility ranges (see Table 2) only the lower end of the distribution is changed while the upper end is always at $1000\,g\,L^{-1}$. The unity activity case displays a much stronger n-dependence (Fig. 9b, based on 3492 points): if analysed separately, the median c_t shifts from about 0.1 to $10\,g\,L^{-1}$ when n changes from 100 to 10 and 5, and up to $100\,g\,L^{-1}$ for $n = 3$. Unlike the ideal mixture this behavior is explained by the actual dissolution thermodynamics: in a system where the components do not affect each other's solubility directly (i.e. the dissolution of a compound i is only limited by its own presence in the aqueous phase), the amount of dissolved material is only dependent on the total water content and is larger the larger the number of dissolvable components. If all the different mixtures are integrated together the median c_t for the unity activity assumption lies at about $1\,g\,L^{-1}$ – a decade lower than for the ideal mixture case.

Figure 10 compares the fitted ε_{eff} values to the fraction of mass with solubilities above the median c_t for the 134 activation points with $s_c = 0.1$, 0.3, 0.6 and 1 %, individually for both organic activity assumptions. The fitted dissolved fraction corresponds well to the fraction of mass with solubilities above the 50 %-partitioning point, as predicted by the theoretical principles outlined in Sect. 2.2.4. Also, the solubilities of the different distributions with varying shapes, numbers of components and solubility ranges can be represented reasonably well with a single median c_t (equal to $10\,g\,L^{-1}$ for the ideal

ACPD
14, 28523–28569, 2014

mixture case and 1 g L^{-1} for the unity activity case, see Fig. 9) with median deviations between the fitted $\varepsilon_{\mathrm{eff}}$ and the fraction above c_{t} of 9 and 8 %, respectively. On the other hand, these results indicate that the soluble fractions determined from experimental data on CCN activation give insight into the fraction of material with solubility above c_{t}. There are 8 points that do not seem to follow the general trend, however: a group of points with all the material above the threshold solubility can display a variety of fitted $\varepsilon_{\mathrm{eff}}$ values. These are all points that correspond to the "high" solubility ranges. Distributions 5 and 6 (see Table 2) with $n = 3$ are among these points for both organic activity assumptions. For the ideal mixture case also distribution 1 with 3 components diverges from the general trend, and for the unity activity assumption distribution 5 falls into the category regardless of the number of components. These points thus contribute to the high ends of the c_{t} distributions in Fig. 9.

Figure 11 displays the deviations in the activation diameters as predicted with the three simplified solubility representations (complete dissolution, ε and κ) as a function of the mixture properties for $s_{\mathrm{c}} = 0.1$, 0.3, 0.6 and 1 %. Again, the two different assumptions about the organic phase activity are treated separately due to their different limiting solubilities c_{t} (Fig. 9) and different shapes of the partitioning distributions (Fig. 8). Also, the points close to complete dissolution at the point of activation ($\varepsilon \geq 0.8$, see Fig. 5 and its explanation in the text) are presented with a different color (gray symbols) than the points where the activation diameter differs significantly from the complete dissolution prediction ($\varepsilon < 0.8$, black symbols). As expected, the complete dissolution assumption performs better the more soluble the organic mixture. Figure 11a and b illustrates this by showing the relationship between the norm of the error in the predicted $D_{\mathrm{p,\,act}}$ and the fraction of material below the median c_{t} (10 and 1 g L^{-1}) for the two organic activity assumptions. The larger the amount of material below the solubility limit, the larger the deviation from the full model predictions. For the κ and ε models, on the other hand, the variable best correlating with the error in $D_{\mathrm{p,\,act}}$ induced by the simplification is different for the different organic activity assumptions – although close to complete dissolution these models also do well, nearly independent of the solubil-

ACPD
14, 28523–28569, 2014

ity of the distribution. For the ideal mixture case the fraction of mass between 1 and 100 g L^{-1} correlates better with the error (Fig. 11c and e) than the mass fraction below any solubility limit (not shown), while for the unity activity case the material at the low end of the distribution (mass fraction below 1 g L^{-1}) performs better (see Fig. 11d and f). The reason for this lies in the different shapes of the partitioning distributions resulting from the two assumptions (Fig. 8). For the symmetric partitioning curve of the ideal mixture case, the predicted ε and κ are most sensitive to differences in the partitioning behaviour between compounds within the range of c_t corresponding to the supersaturation and particle diameter ranges studied here, i.e. 1–100 g L^{-1} (see Fig. 11c and e). Anything outside these boundaries will behave as completely soluble or insoluble throughout the studied supersaturation space, thus not introducing a significant error when constant ε is assumed to describe the mixture. However, the more the material that can behave as either insoluble or soluble depending on the conditions, the larger error we introduce by assuming a constant ε for a given mixture at any conditions. The story is different for the unity activity case (Figs. 11d and f): as the shape of the partitioning distribution (Fig. 8) does not depend on c_t, the compounds with solubilities below c_t will contribute relatively much more the fitted ε_{ff} than for the previous case, and thus the more material there is in the "tail" of the partitioning distribution, the worse the assumption about a single ε for the whole distribution.

4 Discussion and conclusions

We have studied the relationship between CCN activation and solubility of 144 different theoretically constructed complex organic mixtures using Köhler theory, accounting for the partial solubility of the compounds in water and assuming ideal interactions with water. The mixtures encompassed a wide variety of solubilities, and were represented by solubility distributions with various solubility ranges and shapes ("The Solubility Basis Set", SBS). Two limiting assumptions (ideal mixture vs. unity activity) about the interactions between the organics in the insoluble organic phase were tested. The results

ACPD
14, 28523–28569, 2014

using this comprehensive solubility representation (termed as "the full model") were compared to commonly-used simplified descriptions of solubility: (1) assuming complete dissolution, (2) representing the mixture with single hygroscopicity parameter κ, (3) representing the mixture with a single soluble fraction $\varepsilon_{\mathrm{eff}}$. The calculations were carried out for particle dry sizes ranging from 20 to 500 nm and supersaturations between 0.03 and 5 %, thus probing an atmospherically representative parameter space and resulting in total 5957 unique activation points.

Comparing the full model predictions to the simplified solubility descriptions, we find that assuming complete dissolution under-predicts the activation diameter up to about a factor of two for the studied mixtures. Our results indicate that about 70–80 % of the material needs be dissolved at the point of activation for the complete dissolution assumption to predict activation diameters that are within 10 % of that produced by the full solubility treatment. Adding a single parameter to describe the mixture solubility improved the situation considerably: the predictions of activation diameters based on a single ε or κ for a given mixture were within 10 % of the full model predictions, the difference between these two approaches being only marginal.

The fitted soluble fractions, $\varepsilon_{\mathrm{eff}}$, describing the solubility distribution (and thus the fitted κ which is directly proportional to ε) were found to correspond well to the fraction of dry particle material with solubilities larger than a given threshold solubility c_{t}. For the ideal organic mixture assumption the median c_{t} was $10\,\mathrm{g\,L^{-1}}$, most of the values falling between 1 and $100\,\mathrm{g\,L^{-1}}$, depending somewhat on the supersaturation. Since the material with solubilities outside this range can generally be treated as completely soluble or insoluble in CCN activation calculations, the error made by using the single soluble fraction increased when a larger fraction of material was present in this critical range. For the unity activity case the median c_{t} was $1\,\mathrm{g\,L^{-1}}$, but decreased with the number of components present in the mixture, n. For the range of $n = 3$–100 studied here, the typical c_{t} values were between 0.1 and $10\,\mathrm{g\,L^{-1}}$. Due to the asymmetric shape of the aqueous-organic phase partitioning of the organics in the unity activity case, the

ACPD
14, 28523–28569, 2014

simplified models performed better, the more material with solubilities larger than c_t was present in the particles.

Our values for the limiting solubilities for complete dissolution are in agreement with the values of 3 and 1 g L^{-1} previously reported by Huff-Hartz et al. (2006) and Chan et al. (2008) based on experimental data on specific mixtures. Our results on the two different assumptions about the organic phase activities indicate that the mixtures investigated by these past studies were probably somewhat non-ideal, where the compounds hindered each other's dissolution less than would be expected for a fully ideal mixture. On the other hand, in light of our findings, the observations on the complete dissolution of aged SOA at CCN activation (Huff Hartz, 2005; Engelhart et al., 2011) indicate that the majority of the material in the studied SOA mixtures had solubilities larger than 10 g L^{-1}. Furthermore, in the κ values of 0.1–0.2 typically observed for SOA (e.g. Duplissy et al., 2011) a large fraction of the detailed information about the mixture solubility is averaged out, due to the contributions of the molar mass and density (and even surface activity) to these values.

Our results suggest that the solubility range corresponding to limited solubility in CCN activation is between 0.1–100 g L^{-1}, and resolving the solubility distributions of aerosol mixtures outside this range gives only little added value for understanding their CCN activation. In fact, this is probably a conservative estimate, as in most cases material below 1 g L^{-1} is practically insoluble and material above 10 g L^{-1} completely soluble – even considering the uncertainty in the organic mixture activity. Furthermore, our results can be used to guide the representation of the cloud activation properties of complex mixtures, and provide quantitative support for the previous notion that knowing the water-soluble fraction of the aerosol mixture in question is the key in most applications. We provide quantitative estimates on how this soluble fraction should be defined in the case of complex mixtures, and when such a simplified model is not expected to perform well. There are, however, some limitations to our approach to keep in mind when applying the results to laboratory experiments or atmospheric data. Since the focus of this work was strictly on the links between solubility and CCN activation, we did

ACPD
14, 28523–28569, 2014

not explore in depth how variation of surface activity, molecular mass, pure-component density, the gas-droplet partitioning of the organic compounds or non-ideality of water with respect to the aqueous phase would affect the results (see also Suda et al., 2012, 2014; Topping et al., 2012). Furthermore, temperature was assumed to stay constant at 298 K. Since many of the thermodynamic properties relevant to CCN activation are temperature dependent (see e.g. Christensen et al., 2012), future work investigating the impact of temperature on the phenomena studied here is needed. Finally, evaluation of the concepts and approaches here (e.g. the solubility limits c_t) with laboratory studies on well-defined complex mixtures over a wide range of solubilities, supersaturations and particle diameters would naturally be warranted.

Acknowledgements. Financial support from the European Research Council project ATMOGAIN (grant 278277), Vetenskapsrådet (grant 2011-5120), the European Commission FP7 integrated project PEGASOS (grant 265148) are gratefully acknowledged.

References

Albrecht, B. A.: Aerosols, cloud microphysics, and fractional cloudiness, Science, 245, 1227–1230, 1989.

Asa-Awuku, A. and Nenes, A.: Effect of solute dissolution kinetics on cloud droplet formation: extended Köhler theory, Geophys. Res., 112, D22201, doi:10.1029/2005JD006934, 2007.

Asa-Awuku, A., Engelhart, G. J., Lee, B. H., Pandis, S. N., and Nenes, A.: Relating CCN activity, volatility, and droplet growth kinetics of β-caryophyllene secondary organic aerosol, Atmos. Chem. Phys., 9, 795–812, doi:10.5194/acp-9-795-2009, 2009.

Asa-Awuku, A., Nenes, A., Gao, S., Flagan, R. C., and Seinfeld, J. H.: Water-soluble SOA from Alkene ozonolysis: composition and droplet activation kinetics inferences from analysis of CCN activity, Atmos. Chem. Phys., 10, 1585–1597, doi:10.5194/acp-10-1585-2010, 2010.

Chan, M. N., Kreidenweis, S. M., and Chan, C. K.: Measurements of the hygroscopic and deliquescence properties of organic compounds of different solubilities in water and their relationship with cloud condensation nuclei activities, Environ. Sci. Technol., 42, 3602–3608, 2008.

ACPD
14, 28523–28569, 2014

Christensen, S. I. and Petters, M. D.: The role of temperature in cloud droplet activation, J. Phys. Chem. A, 116, 9706–17, doi:10.1021/jp3064454, 2012.
Cruz, C. N. and Pandis, S. N.: A study of the ability of pure secondary organic aerosol to act as cloud condensation nuclei, Atmos. Environ., 31, 2205–2214, doi:10.1016/S1352-2310(97)00054-X, 1997.
Cruz, C. N. and Pandis, S. N.: The effect of organic coatings on the cloud condensation nuclei activation of inorganic atmospheric aerosol, J. Geophys. Res., 103, 13 111–13 123, 1998.
Donahue, N. M., Robinson, A. L., Stanier, C. O., and Pandis, S. N.: Coupled partitioning, dilution, and chemical aging of semivolatile organics, Environ. Sci. Technol., 40, 2635–2643, 2006.
Donahue, N. M., Epstein, S. A., Pandis, S. N., and Robinson, A. L.: A two-dimensional volatility basis set: 1. organic-aerosol mixing thermodynamics, Atmos. Chem. Phys., 11, 3303–3318, doi:10.5194/acp-11-3303-2011, 2011.
Donahue, N. M., Kroll, J. H., Pandis, S. N., and Robinson, A. L.: A two-dimensional volatility basis set – Part 2: Diagnostics of organic-aerosol evolution, Atmos. Chem. Phys., 12, 615–634, doi:10.5194/acp-12-615-2012, 2012.
Duplissy, J., Gysel, M., Alfarra, M. R., Dommen, J., Metzger, A., Prevot, S. H., Weingartner, E., Laaksonen, A., Raatikainen, T., Good, N., Turner, S. F., McFiggans, G., and Baltensperger, U.: Cloud forming potential of secondary organic aerosol under near atmospheric conditions, Geophys. Res. Lett., 35, L03818, doi:10.1029/2007GL031075, 2008.
Duplissy, J., DeCarlo, P. F., Dommen, J., Alfarra, M. R., Metzger, A., Barmpadimos, I., Prevot, A. S. H., Weingartner, E., Tritscher, T., Gysel, M., Aiken, A. C., Jimenez, J. L., Canagaratna, M. R., Worsnop, D. R., Collins, D. R., Tomlinson, J., and Baltensperger, U.: Relating hygroscopicity and composition of organic aerosol particulate matter, Atmos. Chem. Phys., 11, 1155–1165, doi:10.5194/acp-11-1155-2011, 2011.
Dusek, U., Frank, G. P., Hildebrandt, L., Curtius, J., Schneider, J., Walter, S., Chand, D., Drewnick, F., Hings, S., Jung, D., Borrmann, S., and Andreae, M. O.: Size matters more than chemistry for cloud-nucleating ability of aerosol particles, Science, 312, 1375–1378, 2006.
Engelhart, G. J., Moore, R. H., Nenes, A., and Pandis, S. N.: Cloud condensation nuclei activity of isoprene secondary organic aerosol, J. Geophys. Res., 116, D02207, doi:10.1029/2010JD014706, 2011.

ACPD
14, 28523–28569, 2014

Goldstein, A. H. and Galbally, I. E.: Known and unexplored organic constituents in the Earth's atmosphere, Environ. Sci. Technol., 41, 1514–1521, 2007.
Good, N., Topping, D. O., Duplissy, J., Gysel, M., Meyer, N. K., Metzger, A., Turner, S. F., Baltensperger, U., Ristovski, Z., Weingartner, E., Coe, H., and McFiggans, G.: Widening the gap between measurement and modelling of secondary organic aerosol properties?, Atmos. Chem. Phys., 10, 2577–2593, doi:10.5194/acp-10-2577-2010, 2010.
Hallquist, M., Wenger, J. C., Baltensperger, U., Rudich, Y., Simpson, D., Claeys, M., Dommen, J., Donahue, N. M., George, C., Goldstein, A. H., Hamilton, J. F., Herrmann, H., Hoffmann, T., Iinuma, Y., Jang, M., Jenkin, M. E., Jimenez, J. L., Kiendler-Scharr, A., Maenhaut, W., McFiggans, G., Mentel, Th. F., Monod, A., Prévôt, A. S. H., Seinfeld, J. H., Surratt, J. D., Szmigielski, R., and Wildt, J.: The formation, properties and impact of secondary organic aerosol: current and emerging issues, Atmos. Chem. Phys., 9, 5155–5236, doi:10.5194/acp-9-5155-2009, 2009.
Hoyle, C. R., Boy, M., Donahue, N. M., Fry, J. L., Glasius, M., Guenther, A., Hallar, A. G., Huff Hartz, K., Petters, M. D., Petäjä, T., Rosenoern, T., and Sullivan, A. P.: A review of the anthropogenic influence on biogenic secondary organic aerosol, Atmos. Chem. Phys., 11, 321–343, doi:10.5194/acp-11-321-2011, 2011.
Huff Hartz, K. E.: Cloud condensation nuclei activation of monoterpene and sesquiterpene secondary organic aerosol, J. Geophys. Res., 110, D14208, doi:10.1029/2004JD005754, 2005.
Huff-Hartz, K. E. H., Tischuk, J. E., Chan, M. N., Chan, C. K., Donahue, N. M., and Pandis, S. N.: Cloud condensation nuclei activation of limited solubility organic aerosol, Atmos. Environ., 40, 605–617, 2006.
Jimenez, J. L., Canagaratna, M. R., Donahue, N. M., Prevot, A. S. H., Zhang, Q., Kroll, J. H., DeCarlo, P. F., Allan, J. D., Coe, H., Ng, N. L., Aiken, A. C., Docherty, K. S., Ulbrich, I. M., Grieshop, A. P., Robinson, A. L., Duplissy, J., Smith, J. D., Wilson, K. R., Lanz, V. A., Hueglin, C., Sun, Y. L., Tian, J., Laaksonen, A., Raatikainen, T., Rautiainen, J., Vaattovaara, P., Ehn, M., Kulmala, M., Tomlinson, J. M., Collins, D. R., Cubison, M. J., Dunlea, E. J., Huffman, J. A., Onasch, T. B., Alfarra, M. R., Williams, P. I., Bower, K., Kondo, Y., Schneider, J., Drewnick, F., Borrmann, S., Weimer, S., Demerjian, K., Salcedo, D., Cottrell, L., Griffin, R., Takami, A., Miyoshi, T., Hatakeyama, S., Shimono, A., Sun, J. Y., Zhang, Y. M., Dzepina, K., Kimmel, J. R., Sueper, D., Jayne, J. T., Herndon, S. C., Trimborn, A. M., Williams, L. R., Wood, E. C., Middlebrook, A. M., Kolb, C. E., Baltensperger, U., and

ACPD
14, 28523–28569, 2014

Worsnop, D. R.: Evolution of organic aerosols in the atmosphere, Science, 326, 1525–1529, doi:10.1126/science.1180353, 2009.
King, S. M., Rosenoern, T., Shilling, J. E., Chen, Q., and Martin, S. T.: Cloud condensation nucleus activity of secondary organic aerosol particles mixed with sulfate, Geophys. Res. Lett., 34, L24806, doi:10.1029/2007GL030390, 2007.
King, S. M., Rosenoern, T., Shilling, J. E., Chen, Q., and Martin, S. T.: Increased cloud activation potential of secondary organic aerosol for atmospheric mass loadings, Atmos. Chem. Phys., 9, 2959–2971, doi:10.5194/acp-9-2959-2009, 2009.
King, S. M., Rosenoern, T., Shilling, J. E., Chen, Q., Wang, Z., Biskos, G., McKinney, K. A., Pöschl, U., and Martin, S. T.: Cloud droplet activation of mixed organic-sulfate particles produced by the photooxidation of isoprene, Atmos. Chem. Phys., 10, 3953–3964, doi:10.5194/acp-10-3953-2010, 2010.
Kreidenweis, S. M., Petters, M. D., and DeMott, P. J.: Deliquescence-controlled activation of organic aerosols, Geophys. Res. Lett., 33, L06801, doi:10.1029/2005GL024863, 2006.
Kroll, J. H., Donahue, N. M., Jimenez, J. L., Kessler, S. H., Canagaratna, M. R., Wilson, K. R., Altieri, K. E., Mazzoleni, L. R., Wozniak, A. S., Bluhm, H., Mysak, E. R., Smith, J. D., Kolb, C. E., and Worsnop, D. R.: Carbon oxidation state as a metric for describing the chemistry of atmospheric organic aerosol, Nature Chem., 3, 133–139, 2011.
Massoli, P., Lambe, A. T., Ahern, A. T., Williams, L. R., Ehn, M., Mikkil A. J., Canagaratna, M. R., Brune, W. H., Onasch, T. B., Jayne, J. T., Petäjä, T., Kulmala, M., Laaksonen, A., Kolb, C. E., Davidovits, P., and Worsnop, D. R.: Relationship between aerosol oxidation level and hygroscopic properties of laboratory generated secondary organic aerosol (SOA) particles, Geophys. Res. Lett., 37, L24801, doi:10.1029/2010GL045258, 2010.
McFiggans, G., Artaxo, P., Baltensperger, U., Coe, H., Facchini, M. C., Feingold, G., Fuzzi, S., Gysel, M., Laaksonen, A., Lohmann, U., Mentel, T. F., Murphy, D. M., O'Dowd, C. D., Snider, J. R., and Weingartner, E.: The effect of physical and chemical aerosol properties on warm cloud droplet activation, Atmos. Chem. Phys., 6, 2593–2649, doi:10.5194/acp-6-2593-2006, 2006.
Petters, M. D. and Kreidenweis, S. M.: A single parameter representation of hygroscopic growth and cloud condensation nucleus activity, Atmos. Chem. Phys., 7, 1961–1971, doi:10.5194/acp-7-1961-2007, 2007.

ACPD
14, 28523–28569, 2014

Petters, M. D. and Kreidenweis, S. M.: A single parameter representation of hygroscopic growth and cloud condensation nucleus activity – Part 2: Including solubility, Atmos. Chem. Phys., 8, 6273–6279, doi:10.5194/acp-8-6273-2008, 2008.
Petters, M. D. and Kreidenweis, S. M.: A single parameter representation of hygroscopic growth and cloud condensation nucleus activity – Part 3: Including surfactant partitioning, Atmos. Chem. Phys., 13, 1081–1091, doi:10.5194/acp-13-1081-2013, 2013.
Petters, M. D., Wex, H., Carrico, C. M., Hallbauer, E., Massling, A., McMeeking, G. R., Poulain, L., Wu, Z., Kreidenweis, S. M., and Stratmann, F.: Towards closing the gap between hygroscopic growth and activation for secondary organic aerosol – Part 2: Theoretical approaches, Atmos. Chem. Phys., 9, 3999–4009, doi:10.5194/acp-9-3999-2009, 2009a.
Petters, M. D., Kreidenweis, S. M., Prenni, A. J., Sullivan, R. C., Carrico, C. M., Koehler, K. A., and Ziemann, P. J.: Role of molecular size in cloud droplet activation, J. Geophys. Res., 114, D07209, doi:10.1029/2008JD011532, 2009b.
Petters, M. D., Carrico, C. M., Kreidenweis, S. M., Prenni, A. J., DeMott, P. J., Collett Jr, J. L., and Hans Moosmüller, H.: Cloud condensation nucleation activity of biomass burning aerosol, J. Geophys. Res., 114, D22205, doi:10.1029/2009JD012353, 2009c.
Poulain, L., Wu, Z., Petters, M. D., Wex, H., Hallbauer, E., Wehner, B., Massling, A., Kreidenweis, S. M., and Stratmann, F.: Towards closing the gap between hygroscopic growth and CCN activation for secondary organic aerosols – Part 3: Influence of the chemical composition on the hygroscopic properties and volatile fractions of aerosols, Atmos. Chem. Phys., 10, 3775–3785, doi:10.5194/acp-10-3775-2010, 2010.
Prenni, A. J., Petters, M. D., Kreidenweis, S. M., DeMott, P. J., and Ziemann, P. J.: Cloud droplet activation of secondary organic aerosol, J. Geophys. Res., 112, D10223, doi:10.1029/2006JD007963, 2007.
Pruppacher, H. R. and Klett, J. D.: Microphysics of Clouds and Precipitation, 954 pp., Kluwer Acad., Norwell, Mass., 1997.
Psichoudaki, M. and Pandis, S. N.: Atmospheric aerosol water-soluble organic carbon measurement: a theoretical analysis, Environ. Sci. Technol., 47, 9791–8, doi:10.1021/es402270y, 2013.
Rastak, N., Silvergren, S., Zieger, P., Wideqvist, U., Ström, J., Svenningsson, B., Maturilli, M., Tesche, M., Ekman, A. M. L., Tunved, P., and Riipinen, I.: Seasonal variation of aerosol water uptake and its impact on the direct radiative effect at Ny-Ålesund, Svalbard, Atmos. Chem. Phys., 14, 7445–7460, doi:10.5194/acp-14-7445-2014, 2014.

ACPD
14, 28523–28569, 2014

Raymond, T. M. and Pandis, S. N.: Cloud activation of single-component organic aerosol particles, J. Geophys. Res., 107(D24), 4787, doi:10.1029/2002JD002159, 2002.
Raymond, T. M. and Pandis, S. N.: Formation of cloud droplets by multicomponent organic particles, J. Geophys. Res., 108, 4469, doi:10.1029/2003JD003503, 2003.
Seinfeld, J. H. and Pandis, S. N.: Atmospheric Chemistry and Physics: From Air Pollution to Climate Change, 3rd edn., John Wiley, New York, 2006.
Shulman, M. L., Jacobson, M. C., Charlson, R. J., Synovec, R. E., and Young, T. E.: Dissolution behavior and surface tension effects of organic compounds in nucleating cloud droplets, Geophys. Res., 23, 277–280, 1996.
Sotiropoulou, R. E. P., Medina, J., and Nenes, A.: CCN predictions: is theory sufficient for assessments of the indirect effect?, Geophys. Res. Lett., 33, L05816, doi:10.1029/2005GL025148, 2006.
Spracklen, D. V., Jimenez, J. L., Carslaw, K. S., Worsnop, D. R., Evans, M. J., Mann, G. W., Zhang, Q., Canagaratna, M. R., Allan, J., Coe, H., McFiggans, G., Rap, A., and Forster, P.: Aerosol mass spectrometer constraint on the global secondary organic aerosol budget, Atmos. Chem. Phys., 11, 12109–12136, doi:10.5194/acp-11-12109-2011, 2011.
Suda, S. R., Petters, M. D., Matsunaga, A., Sullivan, R. C., Ziemann, P. J., and Kreidenweis, S. M.: Hygroscopicity frequency distributions of secondary organic aerosols, J. Geophys. Res., 117, D04207, doi:10.1029/2011JD016823, 2012.
Suda, S. R., Petters, M. D., Yeh, K., Strollo, C., Matsunaga, A., Faulhaber, A., Ziemann, P. J., Prenni, A. J., Carrico, C. M., Sullivan, R. C., and Kreidenweis, S. M.: Influence of functional groups on organic aerosol cloud condensation nucleus activity, Environ. Sci. Technol., 48, 10182–10190, doi:10.1021/es502147y, 2014.
Swietlicki, E., Hansson, H.-C., Hämeri, K., Svenningsson, B., Massling, A., Mcfiggans, G., Mcmurry, P. H., Petäjä, T., Tunved, P., Gysel, M., Topping, D., Weingartner, E., Baltensperger, U., Rissler, J., Wiedensohler, A., and Kulmala, M.: Hygroscopic properties of submicrometer atmospheric aerosol particles measured with H-TDMA instruments in various environments a review, Tellus B, 60B, 432–469, doi:10.1111/j.1600-0889.2008.00350.x, 2008.
Topping, D. O. and McFiggans, G.: Tight coupling of particle size, number and composition in atmospheric cloud droplet activation, Atmos. Chem. Phys., 12, 3253–3260, doi:10.5194/acp-12-3253-2012, 2012.
Twomey, S.: Pollution and the planetary albedo, Atmos. Environ., 8, 1251–1256, 1974.

ACPD
14, 28523–28569, 2014

VanReken, T. M., Ng, N. L., Flagan, R. C., and Seinfeld, J. H.: Cloud condensation nucleus activation properties of biogenic secondary organic aerosol, J. Geophys. Res., 110, D07206, doi:10.1029/2004JD005465, 2005.

Varutbangkul, V., Brechtel, F. J., Bahreini, R., Ng, N. L., Keywood, M. D., Kroll, J. H., Flagan, R. C., Seinfeld, J. H., Lee, A., and Goldstein, A. H.: Hygroscopicity of secondary organic aerosols formed by oxidation of cycloalkenes, monoterpenes, sesquiterpenes, and related compounds, Atmos. Chem. Phys., 6, 2367–2388, doi:10.5194/acp-6-2367-2006, 2006.

Volkamer, R., Jimenez, J. L., San Martini, F., Dzepina, K., Zhang, Q., Salcedo, D., Molina, L. T., Worsnop, D. R., and Molina, M. J.: Secondary organic aerosol formation from anthropogenic air pollution: rapid and higher than expected, Geophys. Res. Lett., 33, L17811, doi:10.1029/2006GL026899, 2006.

Wex, H., Petters, M. D., Carrico, C. M., Hallbauer, E., Massling, A., McMeeking, G. R., Poulain, L., Wu, Z., Kreidenweis, S. M., and Stratmann, F.: Towards closing the gap between hygroscopic growth and activation for secondary organic aerosol: Part 1 – Evidence from measurements, Atmos. Chem. Phys., 9, 3987–3997, doi:10.5194/acp-9-3987-2009, 2009.

Zieger, P., Weingartner, E., Henzing, J., Moerman, M., de Leeuw, G., Mikkilä, J., Ehn, M., Petäjä, T., Clémer, K., van Roozendael, M., Yilmaz, S., Frieß, U., Irie, H., Wagner, T., Shaiganfar, R., Beirle, S., Apituley, A., Wilson, K., and Baltensperger, U.: Comparison of ambient aerosol extinction coefficients obtained from in-situ, MAX-DOAS and LIDAR measurements at Cabauw, Atmos. Chem. Phys., 11, 2603–2624, doi:10.5194/acp-11-2603-2011, 2011.

ACPD
14, 28523–28569, 2014

Table 1. Simplified descriptions of organic mixture solubilities.

Mixture model	Number of components	Solubility Presentation	Other input parameters
Complete dissolution	1	$c_{sat} \rightarrow \infty^*$	M_{org}, ρ_{org}, σ_{org},
Hygroscopicity κ	1	$\kappa(c_{sat}, M_{org}, \rho_{org})$	–
Soluble fraction ε_{eff}	2	$c_{sat,1} \rightarrow \infty$ $c_{sat,2} = 0$	M_{org}, ρ_{org}

* c_{sat} the solubility (saturation concentration) in aqueous solution.

ACPD
14, 28523–28569, 2014

Table 2. Solubility distributions of the organic mixtures considered in this study.

Distribution[1]	Shape	Number of components	$[c_{sat,\,min}, c_{sat,\,max}]$[2] ($g\,L^{-1}$)
1	Flat, log c axis		
2	Flat, linear c axis		
3	Log. increasing	3, 5, 10, 100	Low: $[10^{-5}, 10^{3}]$
4	Linear increasing		Mid: $[0.1, 10^{3}]$
5	Log. decreasing		High: $[10, 10^{3}]$
6	Linear decreasing		

[1] For all solubility distributions two assumptions about the organic phase activity coefficients: (1) ideal mixture and (2) unity activity (see text for details).
[2] c_{sat} the solubility (pure component saturation concentration) in aqueous solution.

ACPD
14, 28523–28569, 2014

Table 3. Properties of water and organic compounds used in Köhler curve calculations (see Eq. 1).

Property (unit)*	Water	Organic *i*
ρ (kg m^{-3})	1000	1500
σ (N m^{-1})	0.073	0.05
M (kg mol^{-1})	0.018	0.18

* These properties were chosen based on literature on the effective molar masses and densities determined for laboratory SOA (Engelhart et al., 2008; Asa-Awuku et al., 2010), and assumed to be same for every organic compound *i*.

ACPD
14, 28523–28569, 2014

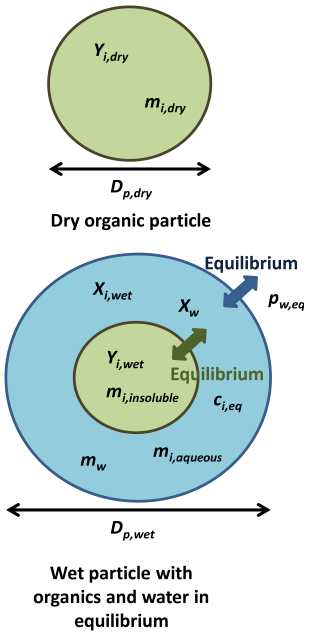

Figure 1. Schematic of the conceptual model used in the equilibrium composition calculations. The dry particle is assumed to consist of n organic compounds, each denoted with a subscript i. The wet particle is assumed to consist of a dry organic (insoluble) phase and an aqueous phase with water and dissolved organics. The aqueous phase is assumed to be in equilibrium with the ambient water vapour. Y refers to mole fractions in the organic phase, X to mole fractions in the aqueous phase, and m to the masses of the organic constituents and water. $c_{i,\,eq}$ refers to the equilibrium concentration of each organic compound in the aqueous solution and $p_{w,\,eq}$ to the equilibrium vapour pressure of water above the aqueous solution.

ACPD
14, 28523–28569, 2014

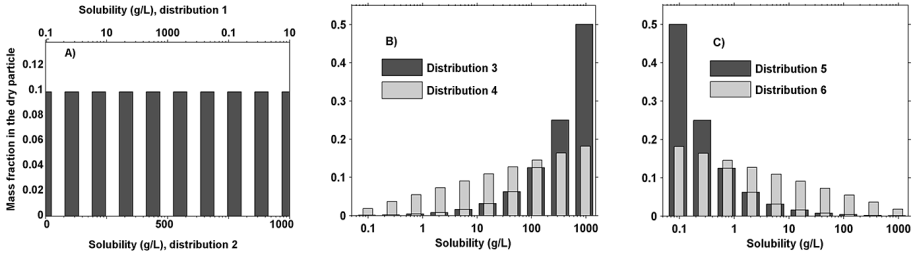

Figure 2. Examples of solubility distributions used in the calculations for saturation concentrations ranging from 0.1 to 1000 $g L^{-1}$. **(a)** Linear and logarithmic flat distributions; **(b)** Linear and logarithmic increasing distributions; **(c)** Linear and logarithmic decreasing distributions. The numbers of the distributions refer to the numbering in Table 2 (see Sect. 2.1.4).

ACPD
14, 28523–28569, 2014

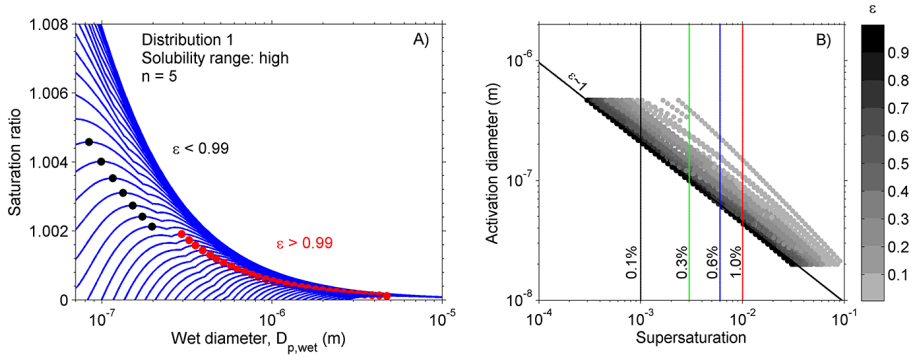

Figure 3. (a) Examples of Köhler curves for the flat logarithmically spaced solubility distribution (Distribution 1 in Table 2) with $n = 5$ and the high solubility range (Table 2). The dots indicate the point of activation, black indicating incomplete dissolution ($\varepsilon < 1$) and red complete dissolution ($\varepsilon = 1$). **(b)** The activation points determined from the model calculations (in total 7200 Köhler curves, see Table 2), corresponding to in total 5957 points in the activation dry diameter vs. supersaturation space. Also the dependence of the dissolved fraction at the point of activation is illustrated.

ACPD
14, 28523–28569, 2014

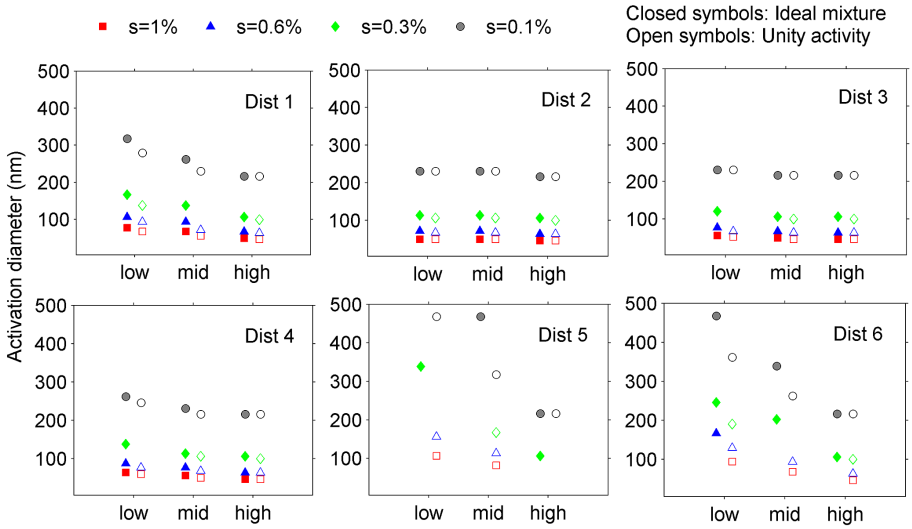

Figure 4. The dependence of the activation diameter for four different supersaturations (s = 1, 0.6, 0.3 and 0.1 %, see also Fig. 3b) on the solubility range for the solubility distributions outlined in Table 2 for n = 5, and the two assumptions about the organic phase activity.

ACPD
14, 28523–28569, 2014

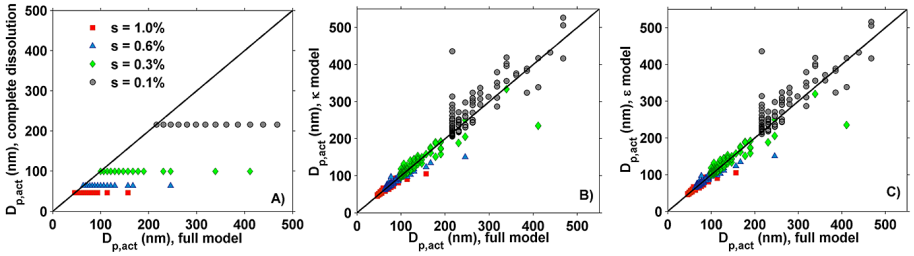

Figure 5. The activation diameter calculated using the solubility distributions (Table 2, referred to as the full model) and the simplified dissolution descriptions (Table 1) **(a)** complete dissolution assumption; **(b)** the hygroscopicity parameter κ; **(c)** the soluble fraction $\varepsilon_{\mathrm{eff}}$ to describe the solubility of the organic mixture. The symbols correspond to the best fits to the full model data. The black line shows the 1 : 1 correspondence between the two data sets.

ACPD
14, 28523–28569, 2014

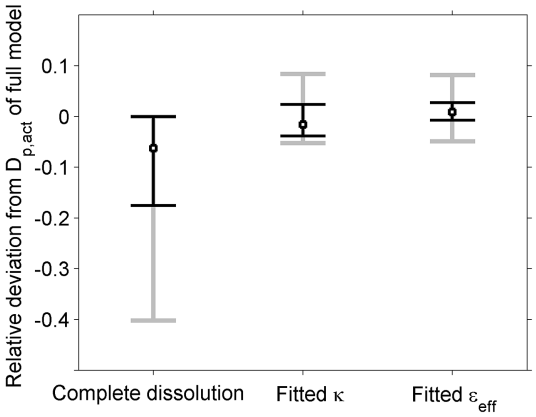

Figure 6. The performance of the simplified solubility representations (see Table 1) in predicting the activation diameter for a given supersaturation as compared with the full model. The black bars depict the 25- and 75-percentiles and the gray bars the 10- and 90-percentiles.

ACPD
14, 28523–28569, 2014

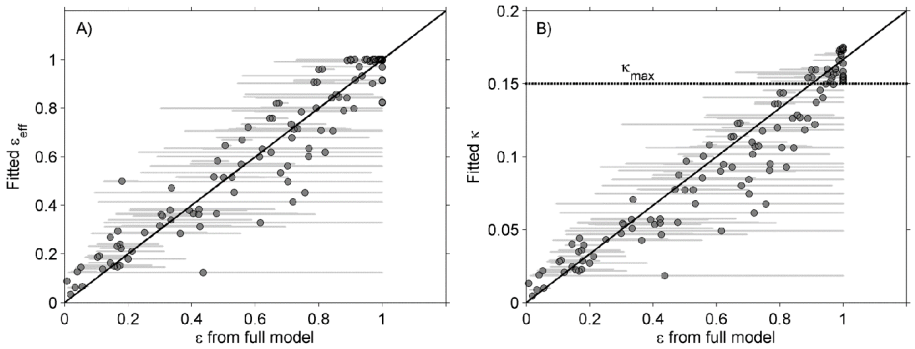

Figure 7. (a) The fitted soluble fraction ε_{eff} as function of the true dissolved fraction ε for each considered mixture (see Table 2). Symbols: mean ε over all activation points. Grey lines: the range of ε values at the different activation points for a given mixture; **(b)** The fitted κ values as a function as function of the true dissolved fraction ε for each considered mixture. The red dashed line denotes the limit of $\kappa_{max} = 0.15$ which applies to all the studied mixtures. 1 : 1 lines are also indicated.

ACPD
14, 28523–28569, 2014

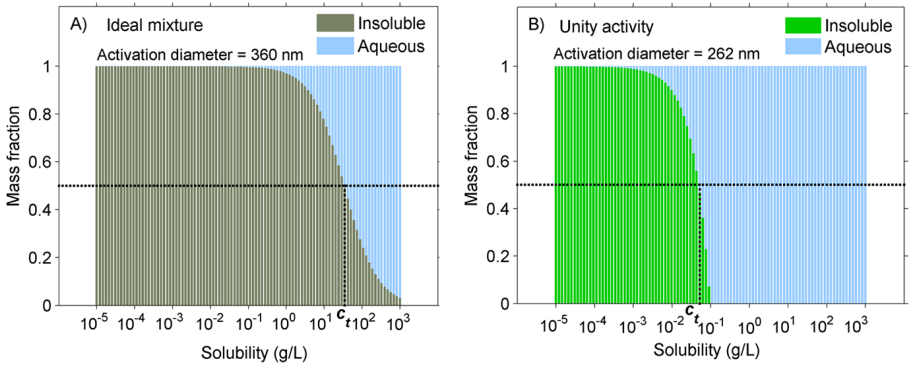

Figure 8. The dissolution behavior of the organic mixture corresponding to Distribution 1 with $n = 100$ and the low solubility range (see Table 2) at the activation point for $s_c = 0.1\,\%$ (see Fig. 4). The figures depict the distribution of material in each solubility bin between the aqueous and the insoluble organic phases for the two different assumptions about the organic phase activity. c_t refers to the 50 %-point of the partitioning (Eq. 22). **(a)** The ideal organic mixture; **(b)** the unity activity assumption.

ACPD
14, 28523–28569, 2014

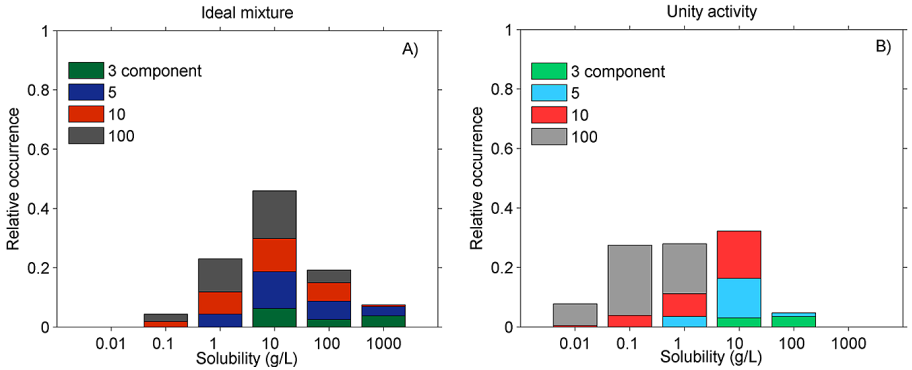

Figure 9. The distributions of the c_t values (i.e. the 50 % partitioning point, see Eq. 22) at the point of activation for all the considered mixtures (Table 2) and activation points, and the two assumptions about the organic phase activity. **(a)** The ideal organic mixture; **(b)** the unity activity assumption.

ACPD
14, 28523–28569, 2014

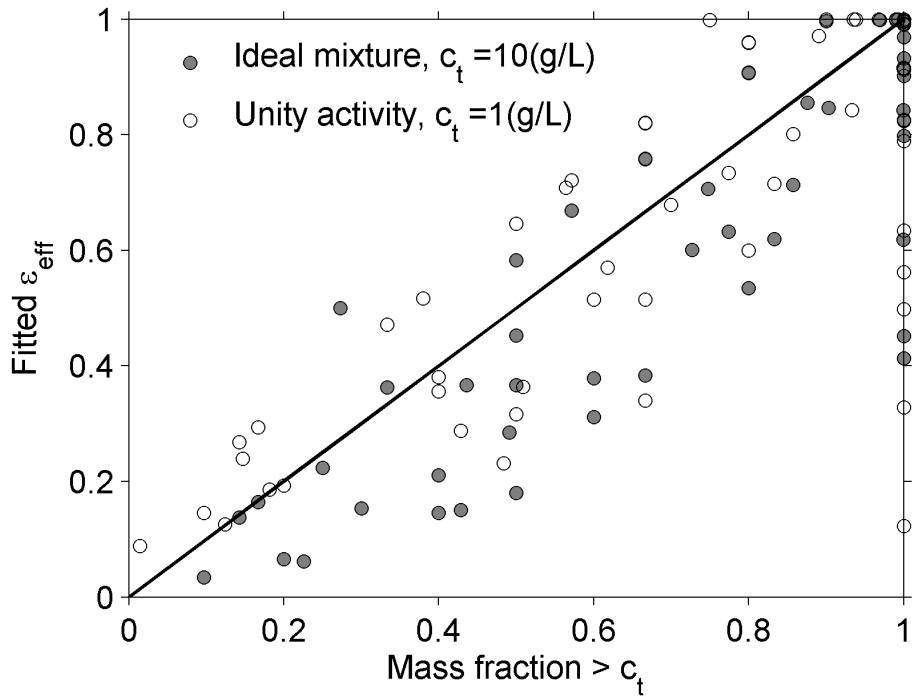

Figure 10. The relationship between the fitted dissolved fraction $\varepsilon_{\mathrm{eff}}$ at the point of activation and the mass fraction over the median c_{t} for all the considered mixtures and $s = 1$, 0.6, 0.3 and 0.1 %. Closed symbols: the ideal organic mixture assumption (median $c_{\mathrm{t}} = 10\,\mathrm{g\,L^{-1}}$). Open symbols: the unity activity assumption for the organics (median $c_{\mathrm{t}} = 1\,\mathrm{g\,L^{-1}}$).

ACPD
14, 28523–28569, 2014

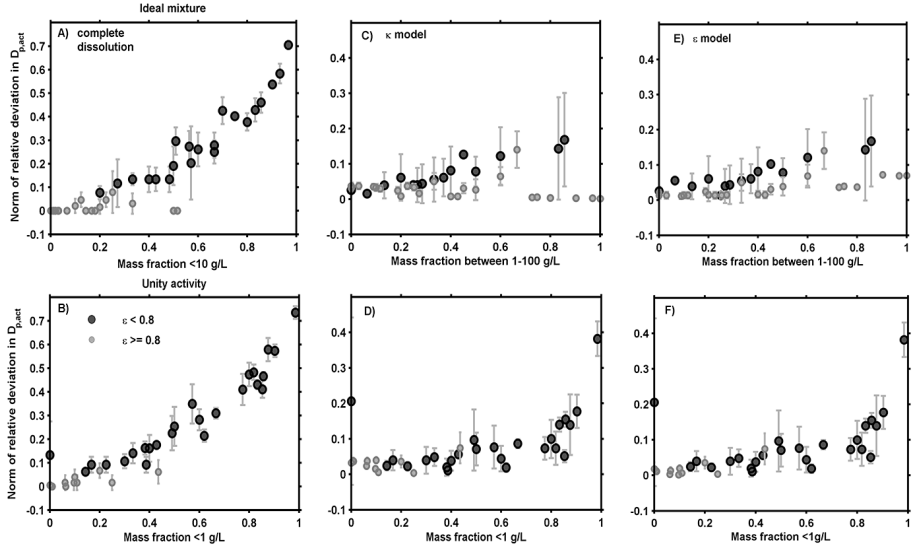

Figure 11. The solubility distribution properties best explaining the performance of the three simplified solubility models, illustrated with the norm of the relative deviation of $D_{p,\,act}$ as compared with the full model predictions for $s = 1$, 0.6, 0.3 and 0.1 %. The performance of the complete dissolution assumption as a function of the mass fraction with solubilities below the median c_t for **(a)** the ideal organic mixture (median $c_t = 10\,g\,L^{-1}$) and **(b)** the unity organic activity (median $c_t = 1\,g\,L^{-1}$) assumptions. The performance of the κ model as a function of the mass fraction with solubilities **(c)** between 1–100 $g\,L^{-1}$ for the ideal organic mixture assumption; **(d)** below 1 $g\,L^{-1}$ for the unity organic activity assumption. The performance of the ε model as a function of the mass fraction with solubilities **(e)** between 1–100 $g\,L^{-1}$ for the ideal organic mixture assumption; **(f)** below 1 $g\,L^{-1}$ for the unity organic activity assumption. The points close to to complete dissolution ($\varepsilon \geq 0.8$) are shown with lighter grey than the rest of the points. The error bars represent the variability with supersaturation and particle size.

ACPD
14, 28523–28569, 2014